Shock Tube Study of the Reaction of CH with N_2: Overall Rate and Branching Ratio

Venkatesh Vasudevan,* Ronald K. Hanson, Craig T. Bowman, David M. Golden, and David F. Davidson

High Temperature Gasdynamics Laboratory, Mechanical Engineering Department, Stanford University, Stanford, California 94305

Received: July 18, 2007; In Final Form: September 6, 2007

We have studied the reaction between CH and N_2, (1) CH + N_2 → products, in shock tube experiments using CH and NCN laser absorption. CH was monitored by continuous-wave, narrow-line-width laser absorption at 431.1 nm. The overall rate coefficient of the CH + N_2 reaction was measured between 1943 and 3543 K, in the 0.9−1.4 atm pressure range, using a CH perturbation approach. CH profiles recorded upon shock-heating dilute mixtures of ethane in argon and acetic anhydride in argon were perturbed by the addition of nitrogen. The perturbation in the CH concentration was principally due to the reaction between CH and N_2. Rate coefficients for the overall reaction were inferred by kinetically modeling the perturbed CH profiles. A least-squares, two-parameter fit of the current overall rate coefficient measurements was $k_1 = 6.03 \times 10^{12}$ exp(−11150/T [K]) (cm^3 mol^{-1} s^{-1}). The uncertainty in k_1 was estimated to be approximately ±25% and approximately ±35% at ∼3350 and ∼2100 K, respectively. At high temperatures, there are two possible product channels for the reaction between CH and N_2, (1a) CH + N_2 → HCN + N and (1b) CH + N_2 → H + NCN. The large difference in the rates of the reverse reactions enabled inference of the branching ratio of reaction 1, $k_{1b}/(k_{1b} + k_{1a})$, in the 2228−2905 K temperature range by CH laser absorption in experiments in a nitrogen bath. The current CH measurements are consistent with a branching ratio of 1 and establish NCN and H as the primary products of the CH + N_2 reaction. A detailed and systematic uncertainty analysis, taking into account experimental and mechanism-induced contributions, yields a conservative lower bound of 0.70 for the branching ratio. NCN was also detected by continuous-wave, narrow-line-width laser absorption at 329.13 nm. The measured NCN time histories were used to infer the rate coefficient of the reaction between H and NCN, H + NCN → HCN + N, and to estimate an absorption coefficient for the NCN radical.

Introduction

The oxides of nitrogen, NO and NO_2 [NO_x], are major atmospheric pollutants. NO_x compounds contribute to acid rain and the destruction of stratospheric ozone and act as facilitators in the production of tropospheric ozone. The primary source of NO_x pollution is through combustion, forming NO, which is then partly converted to NO_2 in the atmosphere. A fundamental understanding of the chemical pathways through which NO_x is produced is important since it is crucial to developing NO_x reduction strategies. There are three major chemical routes to NO formation in combustion: (a) the oxidation of molecular nitrogen, called thermal-NO, (b) the oxidation of nitrogen-containing compounds in the fuel, and (c) NO initiated by the reaction of hydrocarbon fuel fragments with molecular nitrogen, called prompt-NO. A detailed description of NO formation via routes a and b is available elsewhere.[1] In this article, we describe kinetic measurements of the initiation reactions that lead to prompt-NO.

The first observation of prompt-NO was made by Fenimore[2] in hydrocarbon flames. In his experiments, Fenimore found that NO formation in the primary reaction zone exceeds that predicted by the thermal-NO mechanism. Fenimore attributed this additional NO formation to the reaction of molecular nitrogen with hydrocarbon fragments

$$CH + N_2 \rightarrow HCN + N \quad (1a)$$

$$C_2 + N_2 \rightarrow CN + CN \quad (2)$$

The products of reactions 1a and 2 are oxidized to form NO via the sequence CN, HCN → NCO → NH → NO.

In their review paper on nitrogen chemistry, Miller and Bowman[1] conclude that the primary initiation pathway in the prompt-NO mechanism is reaction 1a, with a minor contribution from reaction 3 at high temperatures

$$C + N_2 \rightarrow CN + N \quad (3)$$

Two high-temperature shock tube studies of reaction 1 have been reported in the literature. In an earlier study from this laboratory, Dean et al.[3] monitored CH, generated via the pyrolysis of methane [CH_4] or ethane [C_2H_6] dilute in argon (C_2H_6/CH_4 → CH_3 → CH), using narrow-line-width ring-dye laser absorption at 431.1 nm. The perturbation in the CH profile upon adding N_2 to the initial reaction mixture was used to infer the rate coefficient of reaction 1a in the 2500−3800 K temperature range. Lindackers et al.[4] monitored N atoms generated behind reflected shock waves in C_2H_6/N_2/Ar mixtures between 2600 and 2900 K using ARAS at 119.9 nm. The N atom profiles were fit to a detailed mechanism to infer k_{1a}. The rate coefficients measured in the two studies (Figure 1) agree moderately at ∼2600 K but diverge at higher temperatures. The measured activation energies are quite different—Dean et al.

* Corresponding author. Tel.: (650) 725-6771; fax: (650) 723-1748; e-mail: venkv@stanford.edu.

10.1021/jp075638c CCC: $37.00
Published on Web 10/25/2007

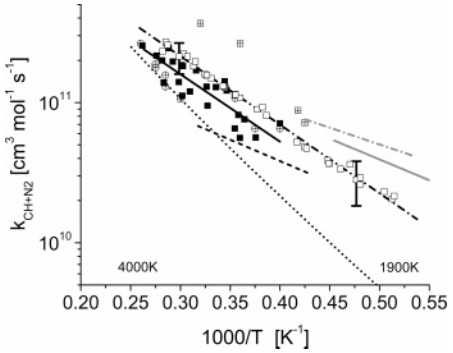

Figure 1. Rate coefficient data for CH + N_2 → products: open squares, this work's data; dashed−dotted black line, this work's fit; solid squares, Dean et al.[3] data; solid black line, Dean et al. fit; dashed line, Lindackers et al.;[4] solid gray line, Matsui et al.;[6] dashed−dotted gray line, Blauwens et al.;[5] crossed circles, Moskaleva and Lin's[12] analysis of the Dean et al. data as measurements of k_{1b}; crossed squares, Moskaleva and Lin's[12] analysis of the Lindackers et al. data as measurements of k_{1b}; and dotted line, Moskaleva and Lin[12] RRKM theory for k_{1b}.

inferred 22 kcal/mol, while Lindackers et al. reported 14 kcal/mol. Because of the difference in the activation energies, an extrapolation of the Arrhenius fits reported in these two studies to flame temperatures leads to rate coefficients that differ by up to a factor of 2. Rate coefficients for reaction 1a have also been inferred indirectly[5,6] from flame experiments. These studies yield higher values of k_{1a} and lower activation energies than the shock tube studies described previously.[7]

While there appears to be a consensus in the literature that the CH + N_2 reaction is the primary initiation step to prompt-NO, there is debate over the products of this reaction. Fenimore[2] postulated the products to be HCN and N, and this was supported by NO measurements in flames[5,6] and limited high-temperature shock tube data.[3,4] However, the formation of HCN and N from CH + N_2 is a spin-forbidden process that requires a potential surface crossing. Several theoretical studies of the spin-forbidden CH + N_2 → HCN + N reaction 1a have been reported in the literature.[8−11] The calculated thermal rate coefficients[9] are much smaller than measured in experiment. Wada and Takayanagi[8] concluded that other mechanisms of prompt-NO formation might be needed to reconcile the serious disagreement between experiment and theory.

Moskaleva and Lin[12] have suggested that the spin-conserved reaction

$$CH + N_2 \rightarrow H + NCN \qquad (1b)$$

is the initiation step in prompt-NO formation at high temperatures rather than the spin-forbidden reaction 1a. The NCN radical is expected to rapidly react with H, O, OH, and O_2 to form intermediates CN, HCN, NH, and NCO that are oxidized to NO. Therefore, the reactions of NCN present additional routes to previously established prompt-NO formation pathways. Moskaleva and Lin have calculated k_{1b} using ab initio methods. Their RRKM rate coefficient expression (dotted line in Figure 1) disagrees with the experimental data of Dean et al.[3] and Lindackers et al.[4]

It is possible to reinterpret existing shock tube measurements of reaction 1a and of the overall reaction rate k_1 as measurements of reaction 1b, as Moskaleva and Lin[12] have done. The results of this analysis, which reflect the current state of rate coefficient measurements for reaction 1b, k_{1b}, are shown in Figure 1. It is evident that there is still a wide variation in k_{1b}, and further work is needed to establish this rate coefficient, especially because of the importance of this reaction in the formation of NO in flames.[13]

At low temperatures (<1000 K), an association/stabilization channel can exist for the CH + N_2 reaction

$$CH + N_2 \rightarrow HCNN \qquad (1c)$$

However, at the temperatures of interest to prompt-NO formation in combustion (>1500 K), and in the temperature and pressure regime where shock tube measurements of the CH + N_2 reaction have been made (1900−4000 K and 0.5−2 atm), this collisionally stabilized process is unimportant, and reactions 1a and 1b are expected to dominate. Measurements of the CH + N_2 reaction have been made at low temperatures and high pressures where the stabilization path is significant and are described elsewhere (see refs 14 and 15 and references cited therein).

Efforts have recently been made to confirm the existence of the spin-allowed NCN channel. Smith[16] and Sutton et al.[17] have detected NCN using laser-induced fluorescence (LIF) in low-pressure hydrocarbon flames. The spatial distribution of the measured NCN LIF signal, its dependence on stoichiometry, its correlation to CH and NO concentration, and its insensitivity to NO addition all are consistent with the premise that it is produced by reaction 1b. Yet, even with these studies, no high-temperature rate coefficient measurements based on NCN data have been performed to date.

Measurements of the reaction product NCN in isolated kinetic experiments would offer stronger evidence for reaction 1b—evidence that is not available by measuring only the reactants, as is evident from the reanalysis of previous shock tube data (see Figure 1). Also, there are no direct measurements of the CH + N_2 rate coefficient at flame temperatures. The uncertainty and scatter in the limited high-temperature data available in the literature is relatively large; this makes a reliable extrapolation of these measurements to flame temperatures difficult. Therefore, the objectives of this work were to (a) perform accurate rate coefficient measurements of reaction 1 over a broad temperature range and (b) establish the product pathways and measure the branching ratio for CH + N_2 → products.

We have made measurements of the overall rate coefficient, k_1, and the branching ratio, $k_{1b}/(k_{1b} + k_{1a})$, of reaction 1 behind reflected shock waves using narrow-line-width CH laser absorption at 431.1 nm. A CH perturbation approach was used to infer k_1 in the 1943−3543 K temperature range. Ethane [C_2H_6] was used as a CH precursor for $T > 2500$ K, while acetic anhydride [$(CH_3CO)_2O$] was used to generate CH for $T < 2500$ K. The effect of the vibrational state of nitrogen ($v = 0$ vs $v = 1$) on the kinetics of the CH + N_2 reaction was also investigated. The branching ratio was inferred in the 2228−2905 K temperature range by shock-heating C_2H_6 dilute in helium and nitrogen. Absorption by NCN was monitored at 329.1 nm, confirming the existence of reaction 1b. In addition, we report rate coefficient data for the reaction between H and NCN between 2378 and 2492 K

$$H + NCN \rightarrow HCN + N \qquad (4)$$

This reaction is thought to be one of the primary routes for NCN removal in hydrocarbon flames. However, its rate coefficient is not well-established, with no previous measurements available in the literature. The rate coefficient was recently calculated by Moskaleva and Lin[12] using ab initio methods. The calculated RRKM rate constant is about a factor of 3 lower than an earlier estimate by Glarborg et al.[21]

All the detailed kinetic model simulations were performed using the CHEMKIN 4.1 software package from Reaction Design. In experiments conducted in a nitrogen bath, the bulk translational temperature changes due to vibrational relaxation. The effect of vibrational cooling was taken into account in the kinetic modeling by imposing a time-dependent temperature profile in CHEMKIN using vibrational relaxation time correlations from Millikan and White.[18,19] As a check on our treatment of the effect of vibrational relaxation on the bulk translational temperature, experiments with added helium were also performed. The addition of helium reduces the vibrational relaxation time. These measurements are described in detail later in the paper. The heat of formation recently measured by Bise et al.[20] for the NCN radical was used in the kinetic modeling.

Experimental Procedures

Shock Tube. All experiments were carried out behind reflected shock waves in a high-purity, stainless steel, helium-driven shock tube with an inner diameter of 14.13 cm. The shock tube facility is described in detail elsewhere.[22,23] Ethane (99%) was obtained from Specialty Chemical Products Inc. and Praxair Inc.; acetic anhydride (99.5%) was obtained from Sigma-Aldrich. Argon (99.9999%), helium (99.999%), and nitrogen (>99%) were supplied by Praxair Inc. Mixtures were made by the method of partial pressures using accurate MKS-Baratron pressure transducers and prepared by successive dilution.[23] The mixtures were allowed to mix overnight in a magnetically stirred mixing chamber to promote homogeneity and consistency before being introduced into the shock tube test section.

The shock tube test section was pumped down to pressures on the order of 10^{-7} Torr before each experiment using mechanical and turbo-molecular pumps. Between experiments, the leak plus outgassing rates were typically less than 10 μTorr/min. Incident shock velocity measurements were made using five PZT pressure transducers and four programmable timer counters and linearly extrapolated to the endwall. Temperature and pressure in the reflected shock region were determined using standard one-dimensional shock relations. Boundary layer and nonideal effects are expected to be negligible because of the large diameter of the shock tube and the relatively short test -times utilized.[24]

CH Absorption. CH radicals were detected by continuous-wave, narrow-line-width ring-dye laser absorption at 431.1 nm. The laser was tuned to the peak of the overlapping $Q_{1d}(7)$ and $Q_{2c}(7)$ rotational lines of the CH A-X (0,0) band.[25] Light at 431.1 nm was generated by pumping Stilbene 3 dye in a Coherent 699 ring-dye laser with the multi-line UV output of a Coherent Innova-200 Ar-ion laser. A Spectra-Physics 470 scanning interferometer was used to check single-mode operation of the dye laser cavity, while the nominal laser wavelength was determined to within ~0.01 cm^{-1} using a Burleigh WA-1000 wavemeter. A multi-line UV beam of ~2.5 W generated ~100 mW visible power at 431 nm. Neutral density filters were used to reduce the power of the beam propagating through the diagnostic section of the shock tube to 1−5 mW. The laser beam was split into diagnostic and reference beams that were balanced prior to each experimental run to provide common-mode rejection of laser intensity fluctuations and a minimum absorption detection limit of less than 0.1%.

Beer's law was used to convert the fractional transmission traces to quantitative CH concentration time histories. Beer's law is given by the relation $(I/I_o)_\nu = \exp(-k_\nu PXL)$, where I is the intensity of the transmitted laser beam and I_o is the intensity of the reference beam, k_ν is the absorption coefficient (atm^{-1} cm^{-1}) at frequency ν, P is the total pressure (atm), X is the mole fraction of the absorbing species, CH, and L is the laser path length (14.13 cm). The absorption coefficient is a function of temperature and pressure and was determined using a spectroscopic model described in detail elsewhere.[25,26a] One of the parameters needed to calculate k_ν is the collision broadening coefficient for CH in the diluent used (argon or nitrogen). The broadening coefficient in argon, $2\gamma_{CH-Ar}$, was recently measured by Vasudevan et al.[25] The collision broadening coefficient of CH in N_2, $2\gamma_{CH-N_2}$, was measured in the present study via repeated single-frequency experiments in shock-heated mixtures of 203.6 ppm ethane in N_2. The measured CH line shape at 2312 K and 4.18 atm was fit to a spectroscopic simulation using LIFBASE;[27] $2\gamma_{CH-N_2}$ (the collision broadened full width at half-maximum, per atm) was used as the fitting parameter. The broadening coefficient of CH in nitrogen was measured to be $2\gamma_{CH-N_2} = 0.044$ cm^{-1} atm^{-1} at 2312 K. The uncertainty in this parameter is conservatively estimated to be ±20%. In absorption coefficient calculations, the temperature dependence used for $2\gamma_{CH-N_2}$ is taken to be the same as that measured for $2\gamma_{OH-N_2}$ by Rea et al.[26b]

NCN Absorption. Although NCN has been observed spectroscopically since the 1960s (see Herzberg and Travis[28]), there has been renewed interest in this radical since the late 1980s because of its appearance in hydrocarbon flames, rockets, and fuel-bound nitrogen combustion. Recent studies by Moskaleva and Lin,[12] Smith,[16] and Sutton et al.[17] have indicated that NCN likely plays an important role in the kinetics of prompt-NO formation.

Spectroscopic studies have been made of the $A^3\Pi - X^3\Sigma$ transition near 329 nm via laser-induced fluorescence in microwave discharges[29,30] and flames.[16,17] However, to the best of our knowledge, laser absorption measurements of NCN have not been performed to date. We have monitored NCN at the A−X (000,000) band head at 329.13 nm via narrow-line-width ring-dye laser absorption. Ultraviolet light near 329 nm was generated using an external-cavity frequency doubler with a BBO nonlinear optical crystal. 658 nm radiation (~200 mW) was first generated in a Coherent 899−21 ring-dye laser cavity, with DCM dye, pumped by a 5 W, 532 nm solid state Spectra-Physics Millenia laser. The visible beam was doubled in an external-cavity, Spectra-Physics WaveTrain, outfitted with a BBO crystal, generating UV light at 329 nm (~15 mW). The UV beam was split into diagnostic and reference beams that were balanced prior to each experiment. This facilitates common-mode rejection of laser intensity fluctuations, leading to a minimum absorption detection limit of less than 0.1%.

The $000\Pi - 000\Sigma$ head in the A−X system was located, and the NCN absorption spectrum was mapped out, both at high and low temperatures, via repeated single-frequency experiments over the 328.5−329.5 nm wavelength range. NCN was generated by heating mixtures of diketene/N_2 and ethane/N_2 behind reflected shock waves. These measurements are shown in Figure 2a,b. The observation of the $010\Delta - 010\Pi$ and $000\Pi - 000\Sigma$ heads at 328.6 and 329.13 nm, respectively, the absence of absorption when nitrogen is replaced with argon, and the qualitative agreement with the NCN LIF excitation spectra of Smith and co-workers[16,29] confirm that the measured absorption is due to the NCN radical. These experiments also confirm that NCN is a product of the reaction between CH and N_2 since it is formed via the following reaction paths: ethane → CH_3 → CH (+N_2) → NCN and diketene → CH_2CO → CH_2 → CH (+N_2) → NCN.

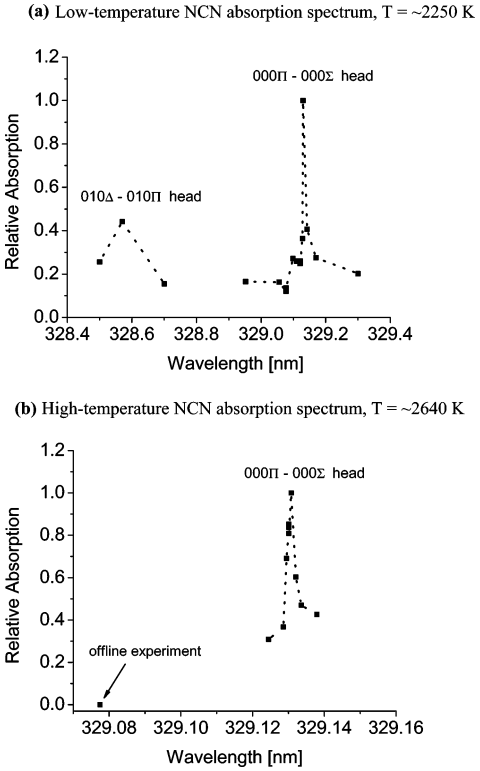

Figure 2. NCN absorption spectrum mapped out via repeated single-frequency experiments at different wavelengths; peak absorption was recorded: (a) measurements between 2215 and 2260 K (frozen *T*) at ~0.82 atm; pre-shock reaction mixture, 253 ppm diketene/N_2; temperature at peak ~2250 K and (b) measurements between 2751 and 2802 K (frozen *T*) at ~0.59 atm; pre-shock reaction mixture, 112.9 ppm ethane/N_2; temperature at peak ~2640 K.

In a subsequent section of this paper, we will demonstrate via careful kinetic experiments and modeling that NCN + H is the dominant (and possibly the only) path of the CH + N_2 reaction.

Overall Rate Coefficient, CH + N_2 → Products. A perturbation approach, similar to that used by Dean et al.,[3] was used to infer the overall rate coefficient for reaction 1, k_1 (where $k_1 = k_{1a} + k_{1b}$). CH was generated by shock-heating different hydrocarbon precursors (ethane, acetic anhydride) dilute in argon. Detailed kinetic mechanisms were developed to model the measured baseline (unperturbed, no N_2 in the reaction mixture) CH concentration time histories. Upon adding nitrogen to the initial reaction mixture, the CH profiles were perturbed, due primarily to the reaction between CH and N_2. Therefore, rate data for reaction 1 could be inferred by adjusting k_1 in the mechanism to best-fit the perturbed CH profiles.

High-Temperature (*T* > 2500 K) Measurements of k_1. At temperatures greater than 2500 K, CH was generated by heating C_2H_6/Ar mixtures behind reflected shock waves. In previous work, different reaction mechanisms were used to model CH formation and removal in hydrocarbon pyrolysis systems. Dean and Hanson[31] used a two-channel mechanism for CH_2 thermal decomposition with nearly equal rate coefficients for the two decomposition pathways, reactions 5a and 5b

$$CH_2 + Ar \rightarrow C + H_2 + Ar \qquad (5a)$$

$$CH_2 + Ar \rightarrow CH + H + Ar \qquad (5b)$$

On the other hand, Kiefer and Kumaran[32] successfully modeled Dean's CH and C atom profiles using a very different reaction mechanism, one consisting primarily of rapid bimolecular reactions. In the Kiefer and Kumaran mechanism, the role of reaction 5b is minimal. That CH_2 decomposition favors reaction 5a was later confirmed by Roth and co-workers.[33]

In recent work,[25] we used a reaction mechanism based on Kiefer and Kumaran to model CH time history measurements in C_2H_6 and CH_3I pyrolysis over a broad temperature and pressure range. The mechanism used in this study to simulate the unperturbed baseline CH profiles is similar to that used in ref 25. Reactions of nitrogen species were added to the mechanism to model the perturbed CH concentration time histories in the presence of N_2. However, as described next, the perturbation in the CH concentration is almost entirely due to reaction 1, facilitating a relatively direct measurement of k_1. Table 1 summarizes the selected rate parameters for the reactions that are important in the high-temperature overall rate coefficient measurements of reaction 1.

An example unperturbed CH concentration time history, resulting from the pyrolysis of 10 ppm ethane dilute in argon, is the upper profile in Figure 3. That the mechanism captures the measured CH profile is evident from the figure. CH is formed primarily from methyl decomposition (reaction 6a)

$$CH_3 + Ar \rightarrow CH + H_2 + Ar \qquad (6a)$$

and is removed by the unimolecular decomposition of CH, reaction 19, and the self-reaction of CH, reaction −21

$$CH + Ar \rightarrow C + H + Ar \qquad (19)$$

$$CH + CH \rightarrow C + CH_2 \qquad (-21)$$

Upon adding 10.1% nitrogen to the initial reaction mixture, the CH profile is perturbed. The perturbed CH time history, with added N_2, is the lower profile in Figure 3. The peak CH mole fraction drops by ~35%. By varying the rate coefficient of only reaction 1 in the mechanism, we can fit the perturbed CH profile (dashed line in Figure 3). For the experiment shown, $k_1 = 2.13 \times 10^{11}$ cm^3 mol^{-1} s^{-1} fits the measurement very well. CH rate of production (ROP) analyses without and with N_2 are shown in Figure 4a,b. As is evident, the only additional CH removal path when N_2 is present is reaction 1. This clearly shows that the perturbation in the CH concentration is principally due to the CH + N_2 reaction. It should be noted that the rates of unimolecular reactions such as CH_3 + M and CH_2 + M change with N_2 addition because of the different third-body collision efficiency of N_2 relative to Ar. However, these changes have no discernible effect on the perturbed CH profiles since the bath gas is primarily argon (added nitrogen was limited to ~10%). The model simulations shown in Figures 3 and 4 have been performed assuming that the only products formed when CH and N_2 react are NCN and H (that this is a good assumption will be demonstrated later in the paper). The choice of product path, however, has no effect on our overall rate coefficient determination—if the products are taken to be HCN and N in the kinetic mechanism, we still obtain the same k_1 value. The current high-temperature measurements of k_1 are summarized in Table 2.

It is important to note that the reaction mechanism used is not unique; however, uniqueness is not essential for a perturbation approach.[31] The only requirement is that the mechanism be applicable both in the presence and in the absence of the perturbing species, which in this case is nitrogen. To check this hypothesis, we used a different set of rate coefficients to model the unperturbed CH profile. For example, the rate coefficient

TABLE 1: Rate Parameters for Reactions Important in CH Perturbation Experiments in Ethane/N_2/Ar

	rate coefficient (cm^3 mol^{-1} s^{-1})			
reaction	*A*	*n*	*E* (kcal/mol)	ref
(1) $CH + N_2 \rightarrow$ products	6.03×10^{12}	0	22.1	this work
(4) $H + NCN \rightarrow HCN + N$	1.89×10^{14}	0	8.4	12[a]
(5a) $CH_2 + M \rightarrow C + H_2 + M$	1.15×10^{14}	0	55.8	32[b]
(5b) $CH_2 + M \rightarrow CH + H + M$	5.60×10^{15}	0	89.6	25
(6a) $CH_3 + M \rightarrow CH + H_2 + M$	3.09×10^{15}	0	80.9	25[b]
(6b) $CH_3 + M \rightarrow CH_2 + H + M$	2.24×10^{15}	0	82.7	25[b]
(11) $CH_2 + H \rightarrow CH + H_2$	1.1×10^{14}	0	0.0	37
(13) $H + CH \rightarrow C + H_2$	1.65×10^{14}	0	0.0	38
(19) $CH + M \rightarrow C + H + M$	1.0×10^{14}	0	64.0	32[b]
(20) $C + CH \rightarrow C_2 + H$	2.0×10^{14}	0	0.0	32
(21) $C + CH_2 \rightarrow 2CH$	1.0×10^{14}	0	0.0	32
(22) $C + CH_3 \rightarrow H + C_2H_2$	5.0×10^{13}	0	0.0	38
(23) $C + CH_4 \rightarrow CH + CH_3$	5.0×10^{13}	0	0.0	32
(24) $CH + CH_3 \rightarrow H + C_2H_3$	6.0×10^{13}	0	0.0	32

[a] Agrees well with the measurements made in the current study. [b] Rate coefficients were adjusted slightly (less than or equal to ±25%) to match each measured baseline CH profile.[25]

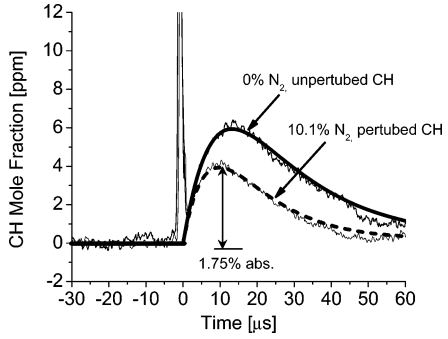

Figure 3. High-temperature CH perturbation experiment: upper CH trace is obtained from the pyrolysis of 10 ppm ethane/Ar at 3348 K and 1.08 atm; lower CH trace is from a similar experiment at 3348 K and 0.95 atm but with 10.1% added N_2; addition of N_2 causes the peak CH mole fraction to be perturbed by ~35%; the solid black and dashed lines are model simulations without and with N_2, respectively; $k_1 = 2.13 \times 10^{11}$ cm^3 mol^{-1} s^{-1} yields a best-fit between the perturbed CH trace and the corresponding numerical simulation.

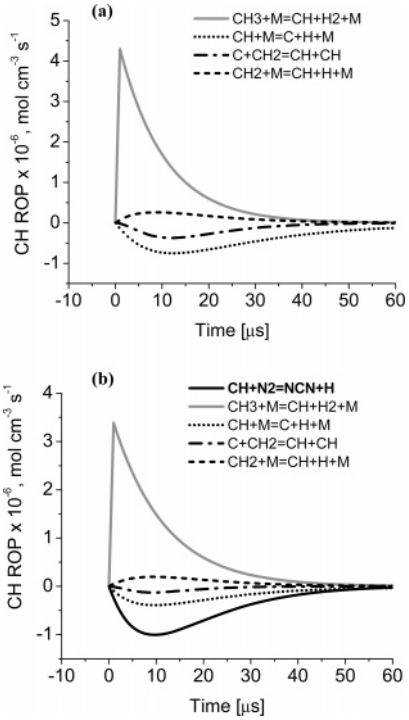

Figure 4. CH ROP at high temperatures: (a) experiment with no N_2, 10 ppm ethane/Ar at 3348 K and 1.08 atm and (b) experiment with added N_2, 10 ppm ethane/Ar/10.1% N_2 at 3348 K and 0.95 atm; the only additional CH removal path in the experiment with added N_2 is the reaction between CH and N_2.

of reaction 6a was adjusted by 25%; to compensate for this change, rate coefficients of other reactions in the base mechanism such as CH + M and CH_2 + M were modified. The k_1 that best-fits the perturbed profile was unchanged (with the modified base mechanism)—this is a direct consequence of the fact that perturbation is due principally to reaction 1. The effect of all the other reactions tends to cancel out across the unperturbed and perturbed CH profiles.

Low-Temperature (T < 2500 K) Measurements of k_1. At temperatures lower than 2500 K, CH was generated by the pyrolysis of acetic anhydride dilute in argon behind reflected shock waves. Akao et al.[34] have studied the thermal decomposition of acetic anhydride behind incident and reflected shock waves at temperatures between 750 and 980 K. The decomposition process was monitored by IR emission at 4.63 μm and vacuum UV absorption at 174.5 nm. The only products observed were acetic acid and ketene

$$(CH_3CO)_2O \rightarrow CH_3COOH + CH_2CO \qquad (7)$$

The reaction was found to be at the high-pressure limit at pressures between 0.16 and 1 atm in the 750−980 K temperature range. The data are in good agreement with earlier measurements carried out in flow and static systems.[35,36] The following Arrhenius expression was reported by Akao et al.: $k_7 = 6.3 \times 10^{11}$ exp(−33 [kcal mol^{-1}]/RT) (s^{-1}).

This Arrhenius expression yields a characteristic decomposition time of less than 6 μs at 1100 K, the typical temperature behind the incident shock in the current experiments. Since the pressure in the present work was always greater than ~0.2 atm, the decomposition proceeds at the high-pressure limit. Therefore, in our experiments, acetic anhydride is expected to rapidly dissociate behind the shock front to form acetic acid (CH_3COOH) and ketene (CH_2CO). The acetic acid then decomposes via two channels

$$CH_3COOH + Ar \rightarrow CH_2CO + H_2O + Ar \qquad (8)$$

$$CH_3COOH + Ar \rightarrow CH_4 + CO_2 + Ar \qquad (9)$$

TABLE 2: Summary of k_1 Measurements at High Temperatures

T (K)[a]	P (atm)[a]	k_1 (cm^3 mol^{-1} s^{-1})
	10.14 ppm C_2H_6, 9.98% N_2, balance Ar	
2819	1.112	1.15×10^{11}
2651	1.199	8.96×10^{10}
2615	1.208	9.29×10^{10}
2916	1.063	1.31×10^{11}
3021	0.975	1.49×10^{11}
3296	0.976	2.23×10^{11}
3503	0.943	2.71×10^{11}
3194	0.892	1.82×10^{11}
	10.04 ppm C_2H_6, 10.1% N_2, balance Ar	
3062	0.979	1.57×10^{11}
3256	0.946	2.14×10^{11}
3175	0.986	1.96×10^{11}
3484	0.918	2.58×10^{11}
3348	0.952	2.13×10^{11}
3543	0.929	2.33×10^{11}
	9.9 ppm C_2H_6, 10.1% N_2, balance Ar	
2778	1.173	1.08×10^{11}
2816	1.121	1.14×10^{11}
2589	1.237	8.11×10^{10}
	10.03 ppm C_2H_6, 10.5% N_2, balance Ar	
2910	1.034	1.30×10^{11}
3080	1.027	1.60×10^{11}
	10.34 ppm C_2H_6, 10.8% N_2, balance Ar	
2901	1.033	1.28×10^{11}

[a] Frozen temperature and pressure, see text.

The ketene formed in reactions 7 and 8 decomposes to form CH_2 and CO

$$CH_2CO + Ar \rightarrow CH_2 + CO + Ar \quad (10)$$

CH is subsequently generated by the rapid reaction of CH_2 and H

$$CH_2 + H \rightarrow CH + H_2 \quad (11)$$

Primary CH removal pathways include the bimolecular reactions of CH with C_2H_2, H, and CH_2

$$CH + C_2H_2 \rightarrow C_3H_2 + H \quad (12)$$

$$CH + H \rightarrow C + H_2 \quad (13)$$

$$CH + CH_2 \rightarrow C_2H_2 + H \quad (14)$$

An acetic anhydride pyrolysis mechanism was assembled to model the measured CH concentration time histories. A ketene pyrolysis mechanism recently reported by Friedrichs and Wagner[37] forms the basis of the current model. Since methane is one of products formed following the initial decomposition of acetic anhydride (reaction 9), reactions from the natural gas oxidation mechanism, GRI Mech 3.0,[38] were added to the Friedrichs mechanism. The important reactions in the mechanism and the rate coefficients used are summarized in Table 3.

A CH sensitivity analysis is presented in Figure 5 for one of the experiments conducted in this study. The CH profile is most sensitive to reactions 10 and 11 and the self-reactions of CH_2

$$CH_2 + CH_2 \rightarrow C_2H_2 + 2H \quad (15)$$

$$CH_2 + CH_2 \rightarrow C_2H_2 + H_2 \quad (16)$$

At later times, the CH profile shows some sensitivity to reactions 12 and 13. The rate coefficients used for reactions 10−13, 15, and 16 are from Friedrichs and Wagner.[37] Small adjustments (<25%) were made to these rate coefficients to best-fit each measured CH trace. For example, the rate coefficients used in this study for reaction 10, ketene decomposition, are in good agreement with previous work[39,40] and only ~20% lower than Friedrichs and Wagner.[37]

As is evident from Figure 5, the CH concentration is also sensitive to the two acetic acid decomposition pathways, reactions 8 and 9, at early times. Only a few studies of acetic acid decomposition have been reported in the literature.[41−44] Mackie and Doolan[41] studied the thermal decomposition of acetic acid dilute in argon in the 1300−1950 K temperature range in a single-pulse shock tube. At a total density of ~1.9 × 10^{-4} mol cm^{-3}, the acetic acid was found to decompose homogenously, with nearly equal rates, via reactions 8 and 9. These measurements are relatively indirect; rate coefficients were inferred by fitting concentration profiles of the residual acid, CH_4, CO_2, and ketene to a detailed kinetic mechanism. Saito et al.[42] investigated the branching ratio of the two competing acetic acid decomposition paths. In the 1300−1800 K temperature range and at a density of 1 × 10^{-5} mol cm^{-3}, the ratio k_9/k_8 was found to be unity. Saito et al. reported rate coefficient expressions at the high-pressure limit, whereas the decomposition is expected to be in the falloff region at the temperatures and pressures that are of interest here. The decomposition of acetic acid is therefore not well-characterized for the experimental conditions used in this work.

In our mechanism (Table 3), we have used high-pressure limit rate coefficients for acetic acid decomposition from a theoretical study by Duan and Page.[43] Fortunately, due to the small sensitivity of the two acetic acid decomposition pathways and because a perturbation approach was used to infer rate coefficient data for k_1, large uncertainties in k_8 and k_9 can be tolerated, with little or no effect on the overall rate coefficient determination for CH + N_2 (this also applies for other reactions in the mechanism such as reactions 15 and 16). This is just an alternate way of stating what was highlighted earlier in the paper—for a perturbation approach, the mechanism used need not be unique; the only requirement is that the mechanism fit the unperturbed CH profile and be applicable both with and without the perturbing species. To confirm that this assumption is valid, for selected experiments, we used a different base mechanism to fit the unperturbed CH profiles. Instead of using acetic acid decomposition rates from Duan and Page,[43] we used rate coefficient expressions from Mackie and Doolan.[41] In the 1900−2500 K temperature range, the Duan and Page rate coefficients for reactions 8 and 9 are 7× and 3.7× the Mackie and Doolan values, respectively. However, since the CH profiles are only weakly sensitive to k_8 and k_9, small changes (<20%) in the rate coefficients of reactions 10 and 11 were sufficient to compensate for the large change in the acetic acid decomposition rates. Upon using the adjusted base mechanism in the perturbation study, the inferred k_1 is unchanged, confirming that the mechanism need not be unique and only needs to fit the unperturbed CH concentration time history.

An example unperturbed CH concentration time history, resulting from the pyrolysis of 25 ppm acetic anhydride dilute in argon, is the upper profile in Figure 6. The mechanism does a very good job of capturing the key characteristics of the CH trace. Upon adding 10.16% N_2 to the initial reaction mixture, the peak CH concentration is perturbed by ~40%; the perturbed CH trace is the lower profile in Figure 6. Figure 7a,b, CH ROP analyses without and with added nitrogen, show that the perturbation in the CH concentration is primarily due to reaction

TABLE 3: Rate Parameters for Reactions Important in CH Perturbation Experiments in Acetic Anhydride/N_2/Ar

	rate coefficient ($cm^3\ mol^{-1}\ s^{-1}$)			
reaction	*A*	*n*	*E* (kcal/mol)	ref
(1) $CH + N_2 \rightarrow$ products	6.03×10^{12}	0	22.1	this work
(4) $H + NCN \rightarrow HCN + N$	1.89×10^{14}	0	8.4	12[a]
(8) $CH_3COOH \rightarrow CH_2CO + H_2O$	2.95×10^{14}	0	78	43[b]
(9) $CH_3COOH \rightarrow CH_4 + CO_2$	7.08×10^{13}	0	74.6	43[b]
(10) $CH_2CO + M \rightarrow CH_2 + CO + M$	9.5×10^{15}	0	58.3	37[c]
(11) $CH_2 + H \rightarrow CH + H_2$	1.1×10^{14}	0	0.0	37[c]
(12) $C_2H_2 + CH \rightarrow C_3H_2 + H$	1.30×10^{14}	0	0.0	37
(13) $H + CH \rightarrow C + H_2$	1.65×10^{14}	0	0.0	38
(14) $CH_2 + CH \rightarrow C_2H_2 + H$	1.00×10^{14}	0	0.0	37
(15) $CH_2 + CH_2 \rightarrow C_2H_2 + 2H$	3.8×10^{14}	0	7.0	37[c]
(16) $CH_2 + CH_2 \rightarrow C_2H_2 + H_2$	3.8×10^{14}	0	7.0	37[c]

[a] Agrees well with the measurements made in the current study. [b] Rate coefficient units: s^{-1}; also see text for explanation on rate coefficient choice. [c] Rate coefficients were adjusted slightly (less than or equal to ±25%) to match each measured CH decay.

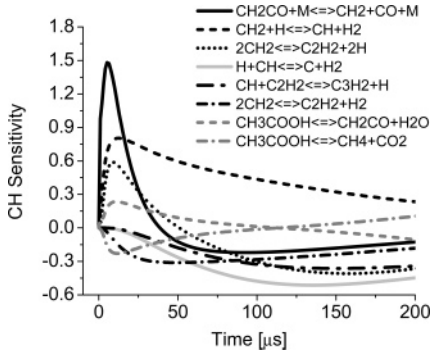

Figure 5. CH sensitivity at low temperatures: 25.77 ppm acetic anhydride/Ar; no N_2 in reaction mixture; initial reflected shock conditions − 2278 K and 1.35 atm.

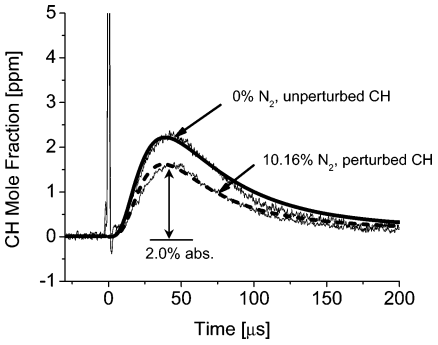

Figure 6. Low-temperature CH perturbation experiment: upper CH trace is obtained from the pyrolysis of 25.77 ppm acetic anhydride/Ar at 2278 K and 1.35 atm; lower CH trace is from a similar experiment at 2233 K and 1.35 atm but with 10.16% added N_2; addition of N_2 causes the peak CH mole fraction to be perturbed by ~40%; the solid black and dashed lines are model simulations without and with N_2, respectively; $k_1 = 3.88 \times 10^{10}\ cm^3\ mol^{-1}\ s^{-1}$ yields a best-fit between the perturbed CH trace and the corresponding numerical simulation.

1. This is because with added nitrogen, the only additional CH removal path is reaction 1. Therefore, as in the high-temperature perturbation experiments in ethane, k_1 was adjusted in the mechanism to fit the perturbed CH profile. In the modeling, NCN and H were assumed to be the only products of reaction 1. The choice of product path has a small effect, <15%, on the k_1 determination at low temperatures and was included as an uncertainty in our measurements. The current low-temperature measurements of k_1 are summarized in Table 4. The k_1 data are reported at frozen conditions since the temperature change due to N_2 relaxation is small—this is described in greater detail in the next section.

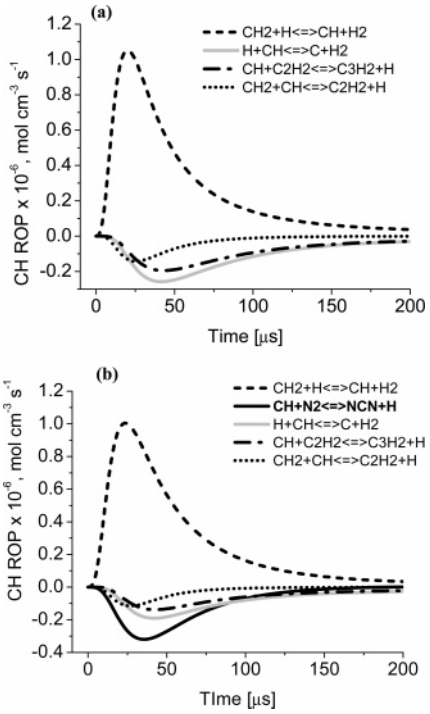

Figure 7. CH ROP at low temperatures: (a) experiment with no N_2, 25.77 ppm acetic anhydride/Ar at 2278 K and 1.35 atm and (b) experiment with added N_2, 25.38 ppm acetic anhydride/Ar/10.16% N_2 at 2233 K and 1.35 atm; the only additional CH removal path in the experiment with added N_2 is the reaction between CH and N_2.

Effect of Vibrational Cooling on Temperature Behind the Reflected Shock Wave. The addition of nitrogen to the reaction mixture in the perturbation experiments causes the test gas to cool in the reflected shock region due to N_2 vibrational relaxation ($V-T$ energy transfer)

$$N_2\ (v = 0) + M \rightarrow N_2\ (v = 1) + M \qquad (17)$$

The vibrational relaxation time, τ_{vib}, can be calculated as a function of temperature and pressure using correlations from Millikan and White.[18] In all our experiments, we limited our data reduction and analysis to a time window over which the temperature change due to relaxation is small. For example, for the high-temperature perturbation experiment shown in Figure 3, the time window of interest is 30 μs ($\Delta T_{0-30\mu s}$ is 1.4%, 47 K), while for the low-temperature perturbation experiment shown in Figure 6, it is 100 μs ($\Delta T_{0-100\mu s}$ is 0.44%, 10 K). The change in the translational temperature of the test gas over the chosen experimental time frame is small, less than 1.5 and 0.5%

TABLE 4: Summary of k_1 Measurements at Low to Moderate Temperatures

T (K)[a]	P (atm)[a]	k_1 (cm^3 mol^{-1} s^{-1})
25.38 ppm acetic anhydride, 10.16% N_2, balance Ar		
2170	1.375	3.36×10^{10}
2233	1.348	3.88×10^{10}
1951	1.405	2.05×10^{10}
2098	1.384	2.82×10^{10}
24.89 ppm acetic anhydride, 10.16% N_2, balance Ar		
2080	1.313	2.91×10^{10}
1981	1.343	2.32×10^{10}
1943	1.391	2.15×10^{10}
2226	1.285	3.67×10^{10}
2356	1.226	4.83×10^{10}
25.46 ppm acetic anhydride, 15.04% N_2, balance Ar		
2082	1.339	2.60×10^{10}
2126	1.301	3.63×10^{10}
2227	1.242	3.68×10^{10}
2398	1.199	5.24×10^{10}
2344	1.228	4.71×10^{10}

[a] Frozen temperature and pressure, see text.

for the high- and low-temperature experiments, respectively. Therefore, we report the current rate coefficient measurements at frozen conditions (Tables 2 and 4). The effect of the change in temperature on the CH concentration profiles was also investigated. A time-dependent temperature profile $T(t)$ was imposed in CHEMKIN to simulate the effect of vibrational cooling. The temperature profile has the following form: $T(t) = T_e + (T_f - T_e)\exp(-t/\tau_{vib})$, where T_e is the vibrationally equilibrated temperature and T_f is the vibrationally frozen temperature. The impact of the temperature change on the CH profile was found to be small (<0.05% absorption). Therefore, the influence of vibrational relaxation on the bulk translational temperature has no discernible effect on our k_1 determination.

Effect of N_2 Vibrational State on CH + N_2 Kinetics. The vibrational state of N_2 ($v = 0$, $v = 1$) could potentially influence the kinetics of the reaction between CH and N_2. At temperatures lower than 2400 K, most of the N_2 is in the $v = 0$ vibrational state in the CH perturbation experiments since the vibrational relaxation time, τ_{vib}, is large in comparison to the time frame of the experiment, τ_{expt}. Also, the population fraction of N_2 in $v = 1$ after vibrational relaxation is fully complete (i.e., at equilibrium) is small, less than 20%. Therefore, it is reasonable to assume that at low temperatures, our measurements are of CH + N_2 ($v = 0$) → products. At higher temperatures, we cannot make this assumption since relaxation is faster and the population fraction in $v = 1$ is higher. Therefore, the effect of the vibrational state of nitrogen on reaction 1 was investigated in experiments with added helium.

An example measurement with helium is shown in Figure 8. Adding 5.7% helium to the argon bath reduces the relaxation time at 2684 K and 1.1 atm from 190 to 25 μs. As a consequence, the fraction of N_2 in $v = 1$ is higher when helium is present in the reaction mixture. In the first 50 μs, the change in the bulk translational temperature for the experiment shown is 2.4% or 65 K. Since the temperature is changing quite rapidly, a time-dependent temperature profile was imposed in CHEMKIN when simulating the measurement. N_2-N_2 and N_2-He relaxation data needed to calculate the temperature profile were taken from refs 18 and 19.

When the experiment with helium was analyzed disregarding the effect of the vibrational state of N_2 on CH + N_2 kinetics, the inferred k_1 value was comparable to that measured in an experiment with no helium. This suggests that the vibrational state of nitrogen does not affect the kinetics of the CH + N_2 reaction, at least to within the resolution of the current experiments. If the N_2 vibrational state did have an effect on k_1, the rate coefficient measured in the experiment with added helium would have been higher or lower than that measured in the experiment with no helium. A similar approach was used in our laboratory to study the OH + CO ($v = 0$, 1) reaction system.[45] In those measurements, the OH + CO reaction rate was found to be dependent on the vibrational state of CO.

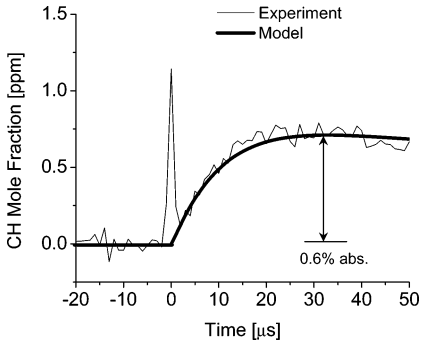

Figure 8. Effect of the vibrational state of nitrogen on k_1; experiment with helium in the reaction mixture: 9.95 ppm ethane/5.72% He/9.98% N_2/Ar; T(frozen) = 2684 K, T(equilibrated) = 2607 K, P = ~1.06 atm; temperature change, due to vibrational relaxation, over 50 μs is 2.4% or 65 K; the best-fit k_1 is unchanged due to helium addition, which indicates that the vibrational state of N_2 does not influence CH + N_2 kinetics.

Branching Ratio Measurements. The branching ratio of reaction 1, $k_{1b}/(k_{1b} + k_{1a})$, was measured by CH laser absorption in experiments in a nitrogen bath. We have taken advantage of the fact that the equilibrium constants of reactions 1a and 1b are very different due to differences in the thermochemical properties of the products formed. As a consequence, reaction −1b, H + NCN → CH + N_2, is orders of magnitude faster than reaction −1a, HCN + N → CH + N_2. The rate coefficient in the forward direction is fixed by the CH perturbation measurements described earlier in the paper. The large difference in the rate coefficients of the reverse reactions results in a strong sensitivity to the branching ratio. For example, the concentration of CH would be higher for a branching ratio of 1 (all H + NCN) than for a branching ratio of 0 (all HCN + N). This is because $k_{-1b} \gg k_{-1a}$, and therefore, more CH is formed when the branching ratio is higher (since the reverse reaction −1b is faster).

Since the branching ratio measurements were made in nitrogen to maximize the effect of the branching ratio on the CH profile, the bulk translational temperature of the test gas changes over the time frame of the experiment due to N_2 vibrational relaxation. The change in temperature due to relaxation was taken into account by imposing a time-dependent temperature profile in CHEMKIN. To calculate the temperature profile, we used vibrational relaxation time correlations from Millikan and White.[18,19]

Dilute mixtures of ethane in nitrogen were shock-heated, and CH was monitored at 431.1 nm. The branching ratio was inferred by fitting the measured CH time histories to detailed kinetic model simulations using the branching ratio as a fitting parameter. An example branching ratio measurement is presented in Figure 9a. We chose to present the measurement in terms of percentage absorption to demonstrate the excellent sensitivity of the CH laser absorption diagnostic (minimum detectable absorption is less than 0.1%). In the kinetic simulation, the concentration profiles output by CHEMKIN were converted to percentage absorption using Beer's law (% absorption = $[1 - \exp(-k_\nu P X_{CH} L)]100$). The temperature

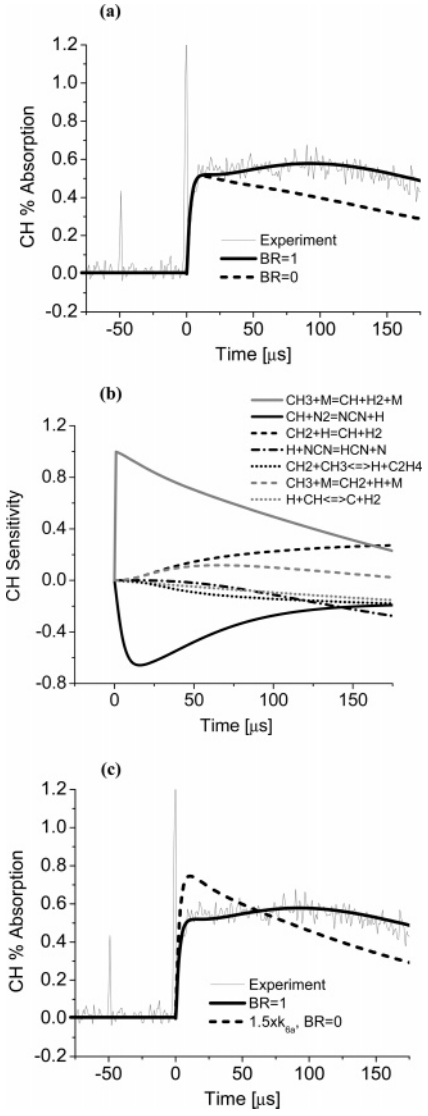

Figure 9. Example CH data, modeling, and sensitivity to infer the branching ratio for $CH + N_2$: (a) CH absorption time history; (b) CH radical sensitivity, $S = (dX_{CH}/dk_i)(k_i/X_{CH})$ and (c) effect of rate coefficient of $CH_3 + M \rightarrow CH + H_2 + M$; 101.39 ppm ethane/$N_2$; T(frozen) = 2634 K, T(equilibrated) = 2249 K, P = ~0.64 atm; temperature drops from 2634 to 2470 K due to vibrational relaxation in 175 μs; data is presented in % absorption to demonstrate the excellent sensitivity of the CH laser absorption diagnostic; minimum detectable absorption is less than 0.1%.

changes by ~145 K over 175 μs due to N_2 vibrational relaxation and was taken into account in the kinetic modeling. The effect of temperature on the CH absorption coefficient, k_ν, was also taken into account.

The chemical kinetic mechanism that was used in the high-temperature perturbation study in ethane was updated and used to model the CH branching ratio measurements. The reactions that are important in the branching ratio experiments are presented in Table 5. Rate coefficients for these reactions were chosen based on a detailed survey of the literature. The rate coefficient used for reaction 1, $CH + N_2 \rightarrow$ products, was from the perturbation experiments described earlier, while rate coefficients for the two methyl decomposition pathways, reactions 6a and 6b, were from Vasudevan et al.[25] The methyl decomposition rates were adjusted to account for the different third-body collision efficiency of nitrogen relative to argon. For reaction 11, $CH_2 + H \rightarrow CH + H_2$, a recent recommendation by Friedrichs and Wagner[37] was used, while for reaction 18, $CH_2 + CH_3 \rightarrow C_2H_4 + H$, we used the Baulch et al.[7] recommendation. Similarly, up-to-date rate coefficients were chosen for the other reactions as well (see Table 5).

The rate coefficients in Table 5 have uncertainty limits, which were determined from the literature. We analyzed all our CH measurements using a range of reasonable rate coefficients that spanned these estimated uncertainty bands. We found that if the rate coefficients for reactions 11 and 4 are ~20% lower and ~50% higher than shown in Table 5, we can fit all our CH absorption profiles to a branching ratio of 1; see, for example, Figure 9a. A branching ratio of 1 is consistent with recent theoretical studies[9,12] of the $CH + N_2$ reaction system. Also, the aforementioned changes in k_{11} and k_4 are well within the uncertainty limits estimated for these reaction rate coefficients. It should be noted that if our CH measurements are analyzed with the rate coefficients shown in Table 5 (i.e., k_{11} and k_4 unchanged), the average branching ratio inferred is 0.88, with estimated upper and lower bounds of 1 (since the branching ratio cannot be greater than 1) and 0.70 (determined using a systematic uncertainty analysis), respectively.

A CH sensitivity analysis for the experiment shown in Figure 9a is presented in Figure 9b. From the CH sensitivity plot, it is evident that the early time jump in CH absorption ($t < 15$ μs) is controlled by the decomposition of methyl radicals to $CH + H_2$, reaction 6a, and the overall $CH + N_2$ rate coefficient, k_1. The collision efficiency of N_2 was adjusted to match the jump in CH absorption at early times. For the low-pressure experiments (~0.6 atm) conducted in this study, a collision efficiency of 1.10−1.15 for N_2 relative to argon best-fits the measured CH jump. At later times, there is sensitivity to reaction 11, $CH_2 + H \rightarrow CH + H_2$, reaction 6b, $CH_3 + M \rightarrow CH_2 + H + M$, reaction 4, $H + NCN \rightarrow HCN + N$, and reaction 18, $CH_2 + CH_3 \rightarrow C_2H_4 + H$.

The CH profile shows good sensitivity to the branching ratio—kinetic model simulations for branching ratios of 0 and 1 are shown in Figure 9a. We have limited ourselves to times <175 μs because the effect of interfering reactions such as $H + NCN \rightarrow HCN + N$ and $CH_2 + H \rightarrow CH + H_2$ become more pronounced at later times (see Figure 9b). Even though the CH profile shows a large sensitivity to reactions 6a and 1, these reactions do not significantly affect our determination of the branching ratio. This is because if either k_{6a} or k_1 is changed, the early time CH jump is not captured. Consequently, the temporal shape of the later time CH profile cannot be reconciled with any branching ratio. This is demonstrated in Figure 9c, where, with $1.5k_{6a}$, even a branching ratio of 0 does not fit the measured CH trace. To confirm that the rate coefficients of reactions 1 and 6a do not have a significant effect on the branching ratio, simulations were performed with different combinations of k_1 and k_{6a}. We found that so long as the early time jump is captured, the branching ratio inferred is the same and not dependent on the k_1 and k_{6a} combination used.

As a check on our treatment of the effect of vibrational relaxation on the bulk translational temperature, experiments with added helium (5 and 10%) were performed. The addition of helium significantly reduces the nitrogen vibrational relaxation time. For example, at 2600 K and 0.6 atm, τ_{vib} with 5% helium is ~50 μs and with 10% helium is ~30 μs, as compared to 250 μs without helium. Experiments were also conducted at higher pressures (2−2.7 atm). Since τ_{vib} scales as $1/P$, the relaxation of nitrogen is faster, and this serves as an additional check on our treatment of N_2 vibrational relaxation. The measurements with and without added helium, at high and low

TABLE 5: Rate Parameters for Reactions Important in Branching Ratio and NCN Time History Measurements

reaction	rate coefficient (cm^3 mol^{-1} s^{-1})			ref
	A	*n*	*E* (kcal/mol)	
(1) CH + N_2 → products	6.03×10^{12}	0	22.1	this work
(4) H + NCN → HCN + N	1.89×10^{14}	0	8.4	12[a]
(6a) CH_3 + M → CH + H_2 + M	see text			25[b]
(6b) CH_3 + M → CH_2 + H + M	see text			25
(11) CH_2 + H → CH + H_2	1.1×10^{14}	0	0.0	37[a]
(13) H + CH → C + H_2	1.65×10^{14}	0	0.0	38
(18) CH_2 + CH_3 → H + C_2H_4	7.2×10^{13}	0	0.0	7
(25) CH_2(S) + H_2 → CH_3 + H	7.0×10^{13}	0	0.0	38
(26) CH_3 + CH_3 → C_2H_5 + H	3.16×10^{13}	0	14.7	46

[a] See text, a 20% lower rate coefficient for k_{11} and a 50% higher rate coefficient for k_4 were used in the branching ratio experiments. [b] Rate coefficient adjusted to match early time CH jump in branching ratio experiments.

TABLE 6: Summary of Branching Ratio Experiments

T(frozen) (K)	*P*(frozen) (atm)	*T*(equilibrated) (K)	*P*(equilibrated) (atm)	*T* over fitting window	av *T* (K)
		103.92 ppm C_2H_6, balance N_2			
2429	0.703	2095	0.676	2429−2268	2349
2443	0.698	2105	0.671	2443−2278	2361
		101.39 ppm C_2H_6, balance N_2			
2548	0.667	2185	0.64	2548−2418	2483
2634	0.641	2249	0.614	2634−2484	2559
2396	0.733	2070	0.705	2396−2228	2312
		101.6 ppm C_2H_6, 5.02% He, balance N_2			
2611	0.598	2241	0.573	2611−2261	2436
		101.09 ppm C_2H_6, 10.02% He, balance N_2			
2671	0.571	2297	0.548	2671−2302	2487
		102.69 ppm C_2H_6, balance N_2			
2531	2.312	2172	2.22	2531−2289	2410
2628	2.182	2244	2.092	2628−2355	2492
		24.88 ppm C_2H_6, 10.2% He, balance N_2			
2905	2.822	2474	2.702	2905−2474	2690
2893	2.738	2465	2.622	2893−2465	2679

pressures, were found to be consistent with one another—a branching ratio of 1 fits all the measured CH profiles.

In summary, CH measurements were performed over a broad range of conditions—pressure, temperature, precursor concentration, helium concentration, and vibrational relaxation time were all varied. The measured CH time histories were fit to the branching ratio of reaction 1 using a detailed kinetic mechanism. A branching ratio of 1 was found to be consistent with all the current measurements. It is important to note that varying reaction rates within their estimated uncertainty limits can lead to lower branching ratios, with a minimum, based on our current understanding of key reactions and rate coefficient uncertainties, of 0.70. Even so, we can conclude that CH + N_2 → NCN + H is the principal pathway for the reaction between CH and N_2. The conditions at which the branching ratio experiments were conducted are summarized in Table 6.

NCN Time History Measurements. NCN absorption time histories were recorded in C_2H_6/N_2 mixtures behind reflected shock waves. NCN was detected at the $A-X$ (000,000) head at 329.13 nm. The experiments were carried out in a nitrogen bath to drive the CH + N_2 reaction forward and to increase the amount of NCN formed. The kinetic mechanism that was used to model the NCN data is the same as that used in the branching ratio experiments. The reactions that NCN is sensitive to are identical to the ones that are important in the branching ratio measurements described earlier and are summarized in Table 5.

An example NCN absorption trace obtained upon shock-heating ethane dilute in nitrogen is presented in Figure 10a. NCN sensitivity and ROP analyses for this experiment are shown in Figure 10b,c, respectively. It is evident from Figure 10c that NCN is formed by the reaction between CH and N_2 and is removed by reaction with H atoms

$$H + NCN \rightarrow HCN + N \quad (4)$$

While NCN formation and removal are principally due to reactions 1 and 4, a complete NCN reaction subset was included in the kinetic mechanism. The NCN reactions and their rate parameters were taken from Moskaleva and Lin.[12]

Since the temperature is changing over the time frame of the experiment due to nitrogen vibrational relaxation (over 300 μs, the bulk translational temperature changes by ~200 K) and because the absorption coefficient of NCN is not known, it is not easy to infer kinetic data from these measurements. However, from Figure 10b, it is evident that the decay in NCN is sensitive principally to reaction 4. This suggests that if we were to conduct experiments where temperature is a constant during the decay period, the effect of the absorption coefficient could be normalized out, facilitating a simple and relatively direct kinetic determination of the rate coefficient of reaction 4. These measurements are described next.

H + NCN → HCN + N. NCN formation and removal, upon shock-heating dilute mixtures of ethane in helium and nitrogen, were measured via laser absorption at 30 383.06 cm^{-1} (329.1307 nm). A relative NCN absorption record (normalized at 100 μs) for an experiment with 10% added helium is shown in Figure 11a. The addition of helium reduces the vibrational relaxation time; the nitrogen relaxes almost completely in ~100 μs. Since at $t > 100$ μs, the temperature is approximately a constant, the decay can be normalized by the NCN absorption level at 100 μs. This removes the effect of the NCN absorption coefficient

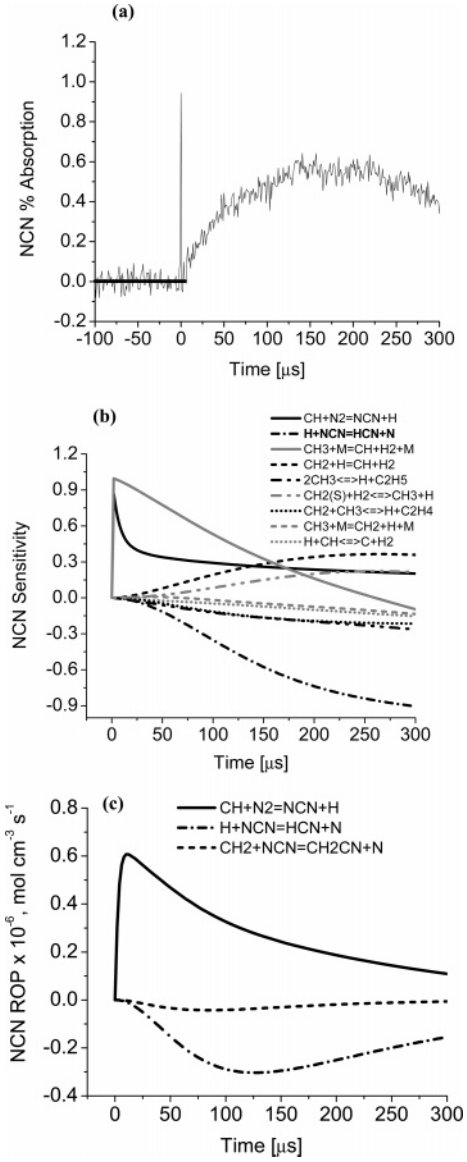

Figure 10. Example NCN absorption data, sensitivity, and ROP: (a) NCN absorption time history, wavenumber is 30 383.12 cm^{-1} (b) NCN radical sensitivity, $S = (dX_{NCN}/dk_i)(k_i/X_{NCN})$ and (c) NCN ROP; 102.23 ppm ethane/N_2; T(frozen) = 2587 K, T(equilibrated) = 2214 K, P = ~0.65 atm; temperature drops from 2587 to 2380 K due to vibrational relaxation in 300 μs.

during the decay period. The various reactions that NCN is sensitive to are shown in Figure 11b. During the decay period, it is evident that reaction 4 has a strong sensitivity, with secondary interference from reactions 1, 6, and 11. The rate coefficient of reaction 4 was adjusted in the mechanism to fit the normalized NCN trace (at $t > 100$ μs). A rate coefficient of 3.45×10^{13} cm^3 mol^{-1} s^{-1} yields an excellent fit between model and experiment. Normalizing the modeled profile with respect to the peak, instead of 100 μs, does not affect our rate coefficient determination.

Measurements for k_4 were conducted over the 2378−2492 K temperature range and are summarized in Table 7 and Figure 12. At lower temperatures, sensitivity to reaction 4 decreases, and secondary chemistry becomes important. At higher temperatures, a large portion of the NCN decay occurs before the test gas has fully relaxed. Hence, it is no longer possible to normalize out the effect of the absorption coefficient as temperature is not a constant during the decay.

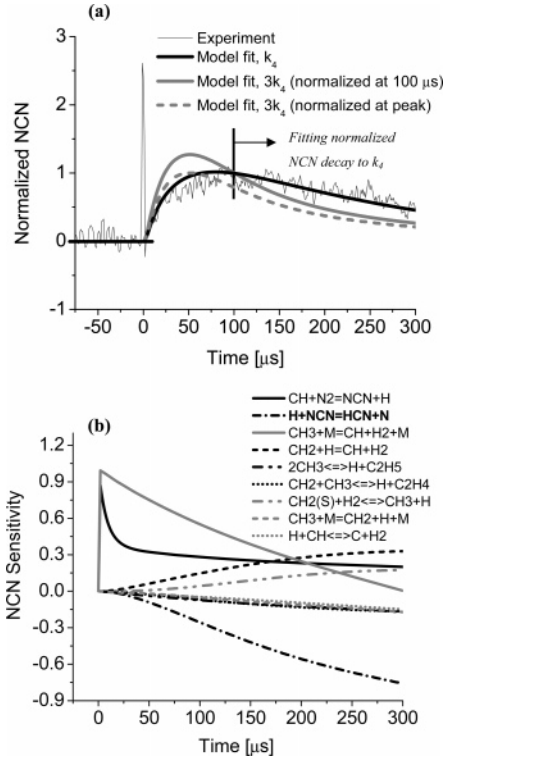

Figure 11. Example experiment to infer k_4: (a) normalized NCN time history, wavenumber is 30 383.06 cm^{-1} and (b) NCN radical sensitivity, $S = (dX_{NCN}/dk_i)(k_i/X_{NCN})$; 105.3 ppm ethane/9.8% He/N_2; T(frozen) = 2930 K, T(equilibrated) = 2492 K, P = ~0.45 atm; test gas is almost completely relaxed in 100 μs.

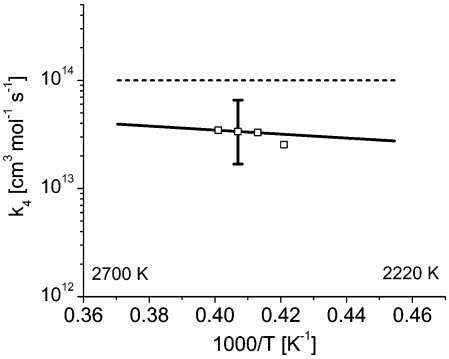

Figure 12. Rate coefficient data for H + NCN → HCN + N: open squares, this work; solid black line, Moskaleva and Lin[12] RRKM theory; dashed line, Glarborg et al.[21] estimate; uncertainty in current data estimated to be a factor of 2.

TABLE 7: Summary of Rate Coefficient Data: H + NCN → HCN + N

T (K)	P (atm)	k_4 (cm^3 mol^{-1} s^{-1})
105.3 ppm ethane, 9.8% He, balance N_2		
2492	0.447	3.45×10^{13}
2455	0.437	3.36×10^{13}
2420	0.413	3.28×10^{13}
101.92 ppm ethane, 10.14% He, balance N_2		
2491	0.401	3.45×10^{13}
2378	0.421	2.54×10^{13}

Our measurement strategy for H + NCN involved the use of normalized NCN profiles. To model NCN absorption quantitatively, the absorption coefficient of NCN, k_{NCN}, is needed as a function of temperature. The absorption coefficient can be inferred approximately from the NCN time histories—the procedure used is described next.

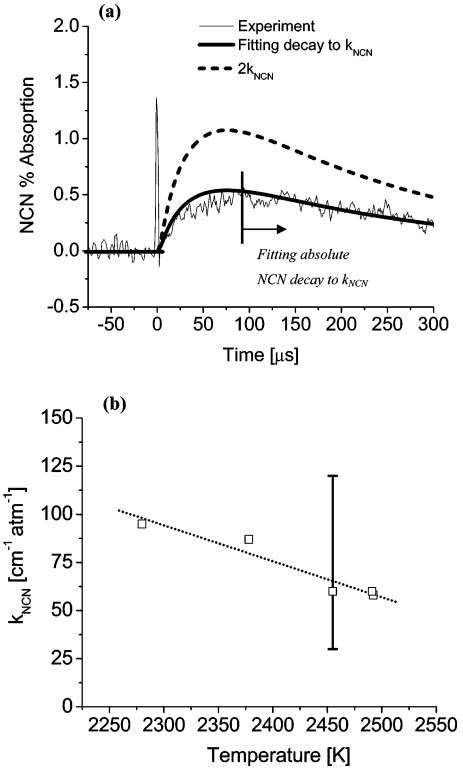

Figure 13. (a) Example experiment to infer the absorption coefficient of NCN; NCN absorption time history at 30 383.06 cm^{-1}; k_{NCN} was adjusted to match NCN decay (best-fit value: 58 cm^{-1} atm^{-1}); 105.3 ppm ethane/9.8% He/N_2; T(frozen) = 2930 K, T(equilibrated) = 2492 K, P = ~0.45 atm; (b) NCN absorption coefficient as a function of temperature; all data inferred with a branching ratio of 1 for reaction 1 in the kinetic mechanism; uncertainty in k_{NCN} is estimated to be a factor of 2.

NCN Absorption Coefficient. We can infer the NCN absorption coefficient, k_{NCN}, in the C_2H_6/He/N_2 experiments used to measure k_4. Figure 13a presents an example measurement. The absorption coefficient of NCN was adjusted to best-fit the absolute, constant-temperature decay in NCN absorption; a simulation with $2k_{NCN}$ is also shown. Over the 2378−2492 K temperature range, at a pressure of ~0.42 atm, k_{NCN} varies between 87 and 55 cm^{-1} atm^{-1}. These values are reasonable and are comparable to previous measurements made in our laboratory for other polyatomic species.[48] For example, the absorption coefficient of NCO[48] varies between 50 and 15 cm^{-1} atm^{-1} in the 2000−2500 K temperature range at ~1 atm. At early times, the fit between model and experiment is poor—this is because at t < 100 μs, the temperature changes significantly due to vibrational relaxation, and the effect of this temperature change on k_{NCN} was not accounted for in the simulations shown in Figure 13a. The current k_{NCN} data are presented as a function of temperature in Figure 13b.

It is important to note that the k_{NCN} measurements are only approximate. From the sensitivity analysis presented in Figure 11b, it is evident that the absolute NCN profile, and therefore the NCN absorption coefficient, is dependent on the rate coefficients of reactions 1, 4, 6, and 11. The primary interfering reaction is that between H and NCN, reaction 4; the uncertainty in the rate coefficient of this reaction is about a factor of 2 (see Results and Discussion). The absorption coefficient is also influenced by the branching ratio of reaction 1. The simulations and k_{NCN} data shown in Figure 13 are for a branching ratio of 1. A branching ratio of 0.85 yields an absorption coefficient that is ~15% higher. Given that there are several error sources (k_1, k_4, k_6, k_{11}, temperature, vibrational relaxation time, and branching ratio), an uncertainty estimate of a factor of 2 for k_{NCN} is reasonable. The primary contributors to the uncertainty are uncertainty in k_4 and k_{11}.

Results and Discussion

In this section, we compare our measurements of k_1, k_4, and the branching ratio with previous work. Detailed uncertainty analyses for our measurements are also described.

Overall Rate Coefficient for CH + N_2. Our measurements of the overall CH + N_2 rate coefficient, k_1, between 1943 and 3543 K in the 0.9−1.4 atm pressure range are presented in Figure 1 (open squares). The current rate coefficient data are in good agreement (to within ~35%) with Dean et al.[3] at high temperatures and have a substantially lower scatter and uncertainty. At temperatures lower than ~2500 K, there are no previous, direct measurements of k_1. Estimates from flame studies exist[5,6] and are shown in Figure 1. Those k_1 values are higher, while the activation energies are lower than measured in this work. All of these previous studies were interpreted as measurements of k_{1a}, CH + N_2 → HCN + N.

The rate coefficient for reaction 1b has been calculated by Moskaleva and Lin[12] using RRKM theory. The calculated rate coefficients do not agree well with the current measurements, particularly at our lowest temperatures. At 2000 K, the calculation is about a factor of 5 smaller than experiment. Recent studies[17] that have attempted to model NO and NCN profiles in low-pressure hydrocarbon flames have found that using the Lin rate coefficient expression leads to an under-prediction of NO and NCN levels in the flame. This observation appears to be consistent with the RRKM rate constant being too low.

A least-squares, two-parameter fit of the current measurements, valid over the 1943−3543 K temperature range, is given by the following expression: $k_1 = 6.03 \times 10^{12} \exp(-11150/T\ [\mathrm{K}])$ (cm^3 mol^{-1} s^{-1}). The correlation coefficient of the fit is −0.98, and the standard deviation is 0.03.

A detailed uncertainty analysis was carried out to set error limits for our measurements of k_1. The uncertainty sources considered were uncertainty in (a) absorption coefficient of CH; (b) initial mixture concentration; (c) reflected shock temperature, primarily due to uncertainty in shock velocity determination; (d) rate coefficients of secondary reactions; (e) choice of product path for reaction 1 in the kinetic modeling; (f) fitting the modeled trace to the experimental profile; and (g) locating time zero. The effect of these uncertainty categories on the rate coefficient of reaction 1 was ascertained and combined via a root-mean-square summation to yield an overall uncertainty estimate for k_1. On the basis of this analysis, we conservatively estimate uncertainties of ±25 and ±35% on our k_1 measurements at ~3350 and ~2100 K, respectively. The primary contributors to the uncertainty are the uncertainty in the reflected shock temperature and the CH absorption coefficient. At low temperatures, uncertainty in fitting the perturbed CH profile to the kinetic model becomes important. This is because the CH profile is only weakly sensitive to the overall rate coefficient at low temperatures.

Branching Ratio for CH + N_2. There have been no previous measurements of the branching ratio of reaction 1. A branching ratio of 1 fits all our CH absorption data, with no discernible dependence on temperature or pressure. Since the branching ratio measurements were made in a nitrogen diluent, the temperature changes in each experiment due to N_2 vibrational relaxation. Table 6 summarizes the experimental conditions at which the branching ratio measurements were made; also shown are the change in temperature due to relaxation and the average

temperature for each experiment. As pointed out earlier, while a branching ratio of 1 is consistent with the current CH measurements, varying key reaction rates within estimated uncertainty limits can lead to lower branching ratios. A detailed and systematic error analysis, taking into account experimental and mechanism-induced contributions, yields a conservative lower bound of 0.70.

Our measurements clearly indicate that the dominant pathway for the $CH + N_2$ reaction is 1b, $CH + N_2 \rightarrow H + NCN$, and confirm the NCN product hypothesis made by Moskaleva and Lin.[12] The current study, in conjunction with a previous flame study by Smith[16] and recent theoretical work on the $CH + N_2$ reaction system,[9,12,47] establishes that NCN is a primary product of reaction 1 and a key precursor to prompt-NO formation.

$H + NCN \rightarrow HCN + N$. The current measurements of k_4 are presented in Figure 12. To the best of our knowledge, this is the first experimental study of reaction 4. The rate data are in excellent agreement with rate coefficients calculated by Moskaleva and Lin[12] using ab initio methods. An estimate by Glarborg et al.[21] is about 3 times the current measurements.

In the 2378−2492 K temperature range, the average rate coefficient measured is $k_4 = 3.2 \times 10^{13}$ cm^3 mol^{-1} s^{-1}. The uncertainty in k_4 is estimated to be about a factor of 2. The primary contributors to this uncertainty are uncertainty in (a) the vibrational relaxation time (and, hence, temperature) and (b) interfering chemistry (here, $CH + N_2 \rightarrow$ products, $CH_3 + M \rightarrow CH + H_2 + M$, and $CH_2 + H \rightarrow CH + H_2$). Since the temperature range of the current experiments is limited and because uncertainty is relatively large, no definitive conclusions can be made regarding the activation energy for reaction 4 based on the measured data.

Conclusion

Sensitive, narrow-line-width laser absorption diagnostics for CH and NCN were used to study the reaction between CH and N_2. The overall rate coefficient was measured in the 1943−3543 K temperature range. The branching ratio was inferred between 2228 and 2905 K, confirming that NCN and H are the principal products of the $CH + N_2$ reaction at combustion temperatures. This observation will impact the modeling of NO formation in hydrocarbon flames since subsequent reactions of NCN will determine the fraction of the NCN that goes on to form NO. The fast back reaction −1b, $H + NCN \rightarrow CH + N_2$, that converts NCN to N_2 competes with reactions that convert NCN to product species that can lead eventually to NO. The present study provides the first high-temperature measurements of the rate coefficient of $NCN + H \rightarrow HCN + N$. Measurements of other NCN removal reactions are needed to provide a complete kinetics model for prompt-NO formation.

Acknowledgment. This work was supported by the Department of Energy, Office of Basic Energy Sciences, with Dr. Frank Tully as contract monitor. The authors thank Dr. Greg Smith (SRI), Dr. Jeffrey Sutton (Naval Research Laboratory), Dr. Jorge Luque (SRI), and Dr. Jay Jeffries (Stanford University) for useful discussions on NCN and CH spectroscopy.

References and Notes

(1) Miller, J. A.; Bowman, C. T. *Prog. Energy Combust. Sci.* **1989**, *15*, 287.
(2) Fenimore, C. P. *Proc. Combust. Inst.* **1971**, *13*, 373.
(3) Dean, A. J.; Hanson, R. K.; Bowman, C. T. *Proc. Combust. Inst.* **1990**, *23*, 259.
(4) Lindackers, D.; Burmeister, M.; Roth, P. *Proc. Combust. Inst.* **1990**, *23*, 251.
(5) Blauwens, J.; Smets, B.; Peeters, J. *Proc. Combust. Inst.* **1977**, *16*, 1055.
(6) Matsui, Y.; Yuuki, A. *Jpn. J. Appl. Phys.* **1985**, *24*, 598.
(7) Baulch, D. L.; Bowman, C. T.; Cobos, C. J.; Cox, R. A.; Just, T.; Kerr, J. A.; Pilling, M. J.; Stocker, D.; Troe, J.; Tsang, W.; Walker, R. W.; Warnatz, J. *J. Phys. Chem. Ref. Data* **2005**, *34*, 757.
(8) Wada, A.; Takayanagi, T. *J. Chem. Phys.* **2002**, *116*, 7065.
(9) Cui, Q.; Morokuma, K.; Bowman, J. M.; Klippenstein, S. J. *J. Chem. Phys.* **1999**, *110*, 9469.
(10) Miller, J. A.; Walch, S. P. *Int. J. Chem. Kinet.* **1997**, *29*, 253.
(11) Rodgers, A. S.; Smith, G. P. *Chem. Phys. Lett.* **1996**, *253*, 313.
(12) Moskaleva, L. V.; Lin, M. C. *Proc. Combust. Inst.* **2000**, *28*, 2393.
(13) Driscoll, J. J.; Sick, V.; Farrow, R. L.; Schrader, P. E. *Proc. Combust. Inst.* **2002**, *29*, 2719.
(14) Berman, M. R.; Lin, M. C. *J. Phys. Chem.* **1983**, *87*, 3933.
(15) Becker, K. H.; Geiger, H.; Wiesen, P. *Int. J. Chem. Kinet.* **1996**, *28*, 115.
(16) Smith, G. P. *Chem. Phys. Lett.* **2003**, *367*, 541.
(17) Sutton, J. A.; Williams, B. A.; Fleming, J. W. *Combust. Flame*, in press.
(18) Millikan, R. C.; White, D. R. *J. Chem. Phys.* **1963**, *39*, 3209.
(19) White, D. R. *J. Chem. Phys.* **1968**, *48*, 525.
(20) Bise, R. T.; Choi, H.; Neumark, D. M. *J. Chem. Phys.* **1999**, *11*, 4923.
(21) Glarborg, P.; Alzueta, M. U.; Dam-Johansen, K.; Miller, J. A. *Combust. Flame* **1998**, *115*, 1.
(22) Vasudevan, V.; Davidson, D. F.; Hanson, R. K.; Bowman, C. T.; Golden, D. M. *Proc. Combust. Inst.* **2007**, *31*, 175.
(23) Herbon, J. T. *Mechanical Engineering Department Report TSD-153, Stanford University*; 2004.
(24) Davidson, D. F.; Hanson, R. K. *Int. J. Chem. Kinet.* **2004**, *36*, 510.
(25) Vasudevan, V.; Hanson, R. K.; Golden, D. M.; Bowman, C. T.; Davidson, D. F. *J. Phys. Chem. A* **2007**, *111*, 4062.
(26) (a) Dean, A. J.; Hanson, R. K. *J. Quant. Spectrosc. Radiat. Transfer* **1991**, *95*, 183. (b) Rea, E. C.; Chang, A. Y.; Hanson, R. K. *J. Quant. Spectrosc. Radiat. Transfer* **1987**, *37*, 117.
(27) Luque, J.; Crosley, D. R. *LIFBASE: Database and Spectral Simulation Program, Version 1.5*; SRI International Report No. MP 99-0099: Menlo Park, California, 1999.
(28) Herzberg, G.; Travis, D. N. *Can. J. Phys.* **1964**, *42*, 1658.
(29) Smith, G. P.; Copeland, R. A.; Crosley, D. R. *J. Chem. Phys.* **1989**, *91*, 1987.
(30) Beaton, S. A.; Ito, Y.; Brown, J. M. *J. Mol. Spectrosc.* **1996**, *178*, 99.
(31) Dean, A. J.; Hanson, R. K. *Int. J. Chem. Kinet.* **1992**, *24*, 517.
(32) Kiefer, J. H.; Kumaran, S. S. *J. Phys. Chem.* **1993**, *97*, 414.
(33) Markus, M. W.; Roth, P.; Tereza, A. M. *Proc. Combust. Inst.* **1994**, *25*, 705.
(34) Akao, M.; Saito, K.; Okada, K.; Takahashi, O.; Tabayashi, K. *Ber. Bunsen-Ges. Phys. Chem.* **1996**, *7*, 1237.
(35) Szwark, M.; Murawski, J. *Trans. Faraday Soc.* **1951**, *47*, 269.
(36) Blake, P. G.; Speis, A. *J. Chem. Soc. B* **1971**, 1877.
(37) Friedrichs, G.; Wagner, H. G. *Z. Phys. Chem.* **2001**, *215*, 1601.
(38) Smith, G. P.; Golden, D. M.; Frenklach, M.; Moriarty, N. W.; Eiteneer, B.; Goldenberg, M.; Bowman, C. T.; Hanson, R. K.; Song, S.; Gardiner, W. C., Jr.; Lissianski, V. V.; Qin, Z.; http://www.me.berkeley.edu/gri_mech/.
(39) Wagner, H. G.; Zabel, F. *Ber. Bunsen-Ges. Phys. Chem.* **1971**, *75*, 114.
(40) Frank, P.; Bhaskaran, K. A.; Just, T. *J. Phys. Chem.* **1986**, *90*, 2226.
(41) Mackie, J. C.; Doolan, J. C. *Int. J. Chem. Kinet.* **1984**, *16*, 525.
(42) Saito, Ko.; Sasaki, T.; Yoshinobu, I.; Imamura, A. *Chem. Phys. Lett.* **1990**, *170*, 385.
(43) Duan, X.; Page, M. *J. Am. Chem. Soc.* **1995**, *117*, 5114.
(44) Blake, P. G.; Jackson, G. E. *J. Chem. Soc. B* **1969**, 94.
(45) Wooldridge, M. S.; Hanson, R. K.; Bowman, C. T. *Proc. Combust. Inst.* **1994**, *25*, 741.
(46) Lim, K. P.; Michael, J. V. *Proc. Combust. Inst.* **1994**, *25*, 713.
(47) Harding, L. B.; Klippenstein, S. J.; Miller, J. A. Submitted to *J. Phys. Chem. A.*
(48) Mertens, J. D.; Dean, A. J.; Hanson, R. K.; Bowman, C. T. *Proc. Combust. Inst.* **1992**, *24*, 701.